

## Spin driving reconstructions on the GaAs(001):Mn surface

S. B. Zhang

National Renewable Energy Laboratory, Golden, Colorado 80401, USA

Lixin Zhang, Lifang Xu, E. G. Wang, Xi Liu, Jin-Feng Jia, and Qi-Kun Xue

State Key Laboratory for Surface Physics and International Center of Quantum Structure, Institute of Physics, Chinese Academy of Sciences, Beijing 100080, China

(Received 13 February 2004; published 25 March 2004)

The scanning tunneling microscopy (STM) experiment reveals a  $2 \times 2$  surface reconstruction on GaAs(001):Mn. A comprehensive theory for spin-driven reconstructions is developed by the first-principles methods: Mn incorporation results in two structural motifs to accommodate the spin degree of freedom. Low-energy reconstructions are generally antiferromagnetic to preserve the semiconducting band gaps. The gaps, however, decrease with increasing Mn coverage, leading to metallic surfaces. At one-monolayer coverage, the transition is complete. The calculated STM images agree with experiment.

DOI: 10.1103/PhysRevB.69.121308

PACS number(s): 68.35.-p, 61.72.Vv, 68.43.-h, 75.70.-i

Understanding epitaxial growth of GaAsMn, a prototype magnetic semiconductor is important for the development of semiconductor-based spintronics.<sup>1-4</sup> On one hand, it is well known that a semiconductor surface, without Mn, is semiconducting by undergoing surface reconstructions<sup>5,6</sup> involving  $sp^2, sp^3, p^3$  local motifs,<sup>7</sup> as conveniently described by an electron-counting (EC) model.<sup>8</sup> On the other hand, due to its active localized  $d$ -orbital, Mn atoms prefer a rather complex pattern of coordination in elemental bulk Mn (a metal) and an eightfold-coordination in MnAs (a semimetal).<sup>9</sup> A central question arises as to what drives the surface reconstruction when Mn is incorporated on the GaAs surfaces. Is the surface stable against phase separation? How would magnetic interaction affect surface reconstruction, and vice versa? How does a semiconductor-to-metal transition take place in such quasi-two-dimensional systems? So far, the study of ferromagnetism in magnetic GaAsMn is focused largely on bulk impurity/defect properties.<sup>10-13</sup> A clear relationship has been demonstrated between magnetic properties and impurities (e.g., substitutional, interstitial, and cluster Mn) and/or native defects (e.g., As antisites). To control and optimize the epitaxial growth of GaAsMn films so as to increase carrier concentration and Curie temperature, however, it is essential to understand Mn-induced surface reconstructions. Recently, it was suggested that surfaces might play a pivotal role in controlling Mn incorporation and site occupation.<sup>13</sup> Yet, very little understanding has been developed for this<sup>13-15</sup> or even for any other semiconductor surfaces involving transition-metal impurities.

In this work we show by combined theoretical and experimental study that, despite the inherent complexity of the magnetic surfaces, spin-driven reconstructions can be understood within a unified simple picture: (a) Low-energy Mn surfaces exist in the form of simple structural motifs. The two basic Mn motifs established in this study are the  $\beta$  motif (interstitial in an  $sd^3$ -like electronic configuration) and the  $\gamma$  motif (“substitutional” in the sense that it replaces a surface-Ga dimer in a  $dsp^2$ -like configuration), shown in Fig. 1. (b) The low-energy surface structures correlate completely with the total magnetic moment ( $M_T$ ) of the unit cell.

If we define the Mn coverage ( $\theta_{\text{Mn}} = n/4$ ),  $M_T$  oscillates between  $5\mu_B/2 \times 2$  for odd  $n$  and 0 for even  $n$ . Accordingly, the low-energy surfaces also oscillate between  $\gamma$ -motif phases for odd  $n$  and  $\beta$ -motif phases for even  $n$ , due to a strong antiferromagnetic coupling for the latter. (c) At low  $\theta_{\text{Mn}}$ , the low-energy surfaces are all semiconducting, facilitated by a universal antiferromagnetic coupling wherever possible. This explains, in accordance with the EC model, why the calculated surface energies are low,  $\sim 0.1 \text{ eV}/(1 \times 1)/\text{Mn}$ . (d) At higher Mn coverages, however, the band gap closes and all

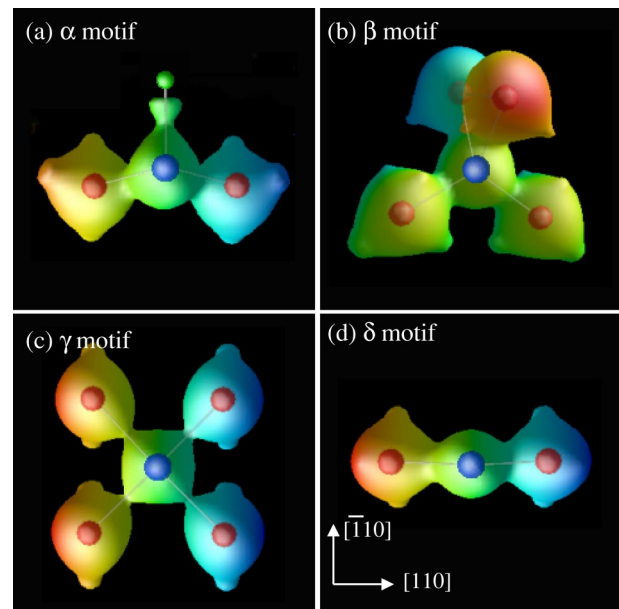


FIG. 1. (Color online) Four Mn structural motifs proposed for the GaAs(001):Mn surface. Large (blue), medium (red), and small (green) balls are the Mn, As, and Ga atoms, respectively. Contour plots show total charge densities near Mn atoms, 10% below the respective maximum value. Lattice directions in (d) apply to (a), (c), and (d), but not (b) in which the  $[110]$  direction points into the paper. Lines connecting atoms may not be the actual chemical bonds.

the surfaces become metallic. The transition is complete at the  $\theta_{\text{Mn}}=1$  monolayer (ML).

Our calculations were performed using the density-functional theory<sup>16</sup> within the general gradient approximation<sup>17</sup> and the Vanderbilt ultrasoft pseudopotentials,<sup>18</sup> as implemented in the VASP code.<sup>19</sup> The Mn and Ga 3*d* states were treated as the valence and core, respectively, and the cutoff energy in the plane-wave expansion is 171 eV. We used an eight-bilayer slab with at least four GaAs bilayers, and the rest is the vacuum. Pseudohydrogen atoms are used to passivate the bottom of the slab. All atoms, except the bottom-layer Ga and H, are fully relaxed until the force is less than 0.1 eV/Å. We used a  $2 \times 2 \times 1$  mesh for the Brillouin-zone integration. Using a 227-eV cutoff energy, or having Ga 3*d* in the valence, yields changes in the relative energy by less than 0.015 eV/(1×1)/Mn, whereas for metallic surfaces, using a  $6 \times 6 \times 1$  mesh yields changes of less than 0.002 eV/(1×1)/Mn.

The energy of a surface *S* relative to the GaAs(001)- $\beta 2(2 \times 4)$  surface is defined as

$$E_S = E_{\text{tot}}(S) - E_{\text{tot}}[\text{GaAs}\beta 2(2 \times 4)] - n_{\text{Ga}}\mu_{\text{Ga}} - n_{\text{As}}\mu_{\text{As}} - n_{\text{Mn}}\mu_{\text{Mn}}, \quad (1)$$

where  $n_i$  is the number of the *i*th atoms ( $i = \text{Ga, As, Mn}$ ) being transferred from a chemical reservoir of energy  $\mu_i$  to the GaAs(001)- $2 \times 4$  surface to form the Mn surface. In general,  $\mu_i$  is a variable bounded below the chemical potential of the corresponding elemental solid, which for convenience is set to zero. Let  $\Delta H_f(\text{GaAs})$  be the formation enthalpy of GaAs. One can show<sup>20</sup> that under equilibrium

$$\mu_{\text{Ga}} = \Delta H_f(\text{GaAs}) - \mu_{\text{As}} \quad (2)$$

and

$$\Delta H_f(\text{GaAs}) \leq \mu_{\text{As}} \leq 0. \quad (3)$$

One can also show that

$$\mu_{\text{Mn}} \leq \min\{\Delta H_f(\text{MnAs}) - \mu_{\text{As}}, 0\}. \quad (4)$$

Otherwise, Mn will phase separate from the surface to form either bulk MnAs or bulk Mn.<sup>21</sup>

GaAs(001) epitaxial layers were grown in a molecular beam epitaxy system and capped with an amorphous As layer. After loading into an UHV STM system, the As capping layer was removed by annealing at 440 °C, resulting in high-quality  $2 \times 4$  reconstruction. Deposition of a small amount of Mn at room temperature (RT) followed by annealing at 390 °C leads to the appearance of depressed  $2 \times 2$  areas, 2.2 Å lower than the original  $2 \times 4$  areas, as indicated by the line scan in Fig. 2(a).<sup>22</sup> Further annealing at 440 °C enlarges the  $2 \times 2$  areas at the expense of the  $2 \times 4$  areas. Figure 2(b) shows a filled-state image at a -2 V bias. Surprisingly, the  $2 \times 2$  surface shows no apparent in-plane atomic displacement, other than a regular vacancy array, in sharp contrast to the (001) surface reconstruction seen for GaAs and other III-V semiconductors.<sup>6</sup>

Figure 3 shows selectively the calculated low-energy structures of the  $2 \times 2$  surfaces. The actual study, however,

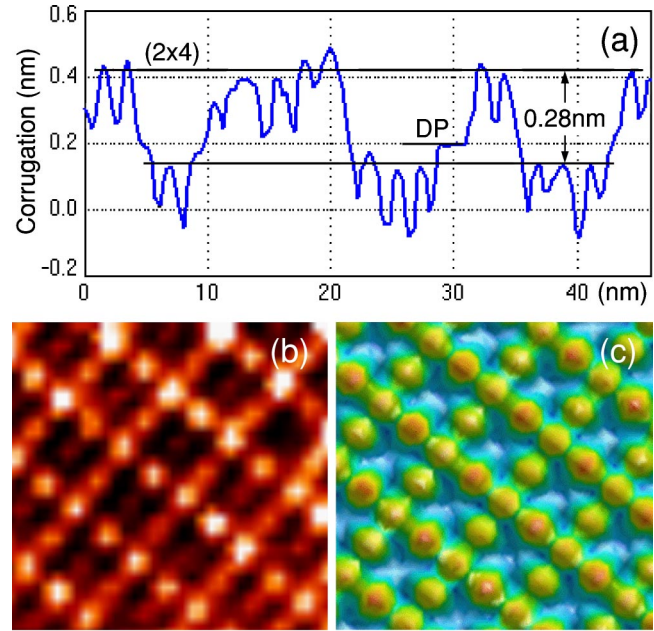


FIG. 2. (Color online) (a) Experimental line scan of the STM image obtained from an As-terminated  $2 \times 4$  and  $2 \times 2$  Mn coexisting area on the GaAs(001):Mn surface. Note that the step height on the GaAs(001) surface, i.e., the distance between the neighboring As (or Ga) layers along the [001] direction, is 0.28 nm. The abbreviation DP indicates the depressed  $2 \times 2$  area. (b) The experimental STM image of the GaAs(001)- $2 \times 2$ :Mn surface at a bias voltage of -2 V (color code: bright is high and dark is low). (c) The calculated STM image at the same bias for the  $\beta_{40-1}$  surface (color code: red is high and blue is low).

covers many more structures drawn from a combination of the four Mn motifs in Fig. 1 (i.e., the  $\beta$  and  $\gamma$  motifs plus the  $\alpha$  and  $\delta$  motifs where the Mn is substitutional with three and two nearest neighbors, respectively) and others that cannot be expressed by this set of motifs; different surface Mn/Ga/As coverage, including surface vacancies; different spin polarization; and different surface terminations, i.e., Ga-, As-, and As double-layer terminated surfaces. Overall, more than eighty surface structures were calculated. We will use the subscript (*lmn*) to indicate surface Mn/Ga/As coverage with respect to the *ideal* As-terminated (001) surface: for example,  $\beta_{100}$  stands for adding one interstitial Mn to the As-terminated surface.

Figure 4 shows the calculated surface energy per  $1 \times 1$  area per Mn as a function of the As chemical potential  $\mu_{\text{As}}$ . Because our primary interest is in the incorporation of Mn into GaAs, here we set  $\mu_{\text{Mn}}$  at its maximum possible thermodynamic value, i.e.,  $\mu_{\text{Mn}} = \Delta H_f(\text{MnAs}) - \mu_{\text{As}}$  for  $\mu_{\text{As}} > \Delta H_f(\text{MnAs})$  and  $\mu_{\text{Mn}} = 0$  otherwise.

$\theta_{\text{Mn}} = 1/4$  ML. Here,  $M_T = 5 \mu_B / 2 \times 2$  for all the cases in Fig. 4(a) except for  $\beta_{11-1}$ . The low-energy structures are the various  $\gamma$  phases. The  $\gamma$  motif can be viewed as having one Mn replace one Ga-Ga dimer on Ga-terminated (001). The Mn assumes a nearly planar geometry with a  $dsp^2$ -like electronic configuration, as depicted in Fig. 1(c). There is a gap between the highest occupied molecular orbital (HOMO) and

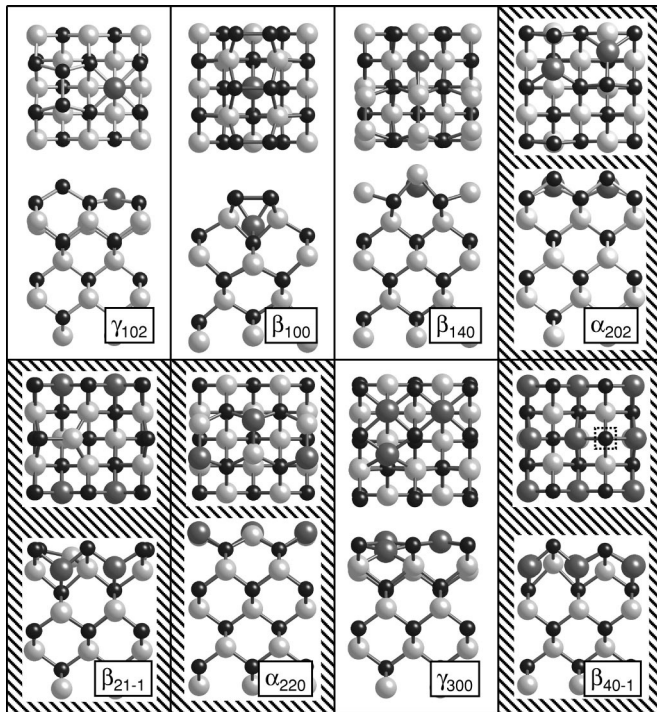


FIG. 3. Top and side views of the calculated low-energy surface structures. Small black balls are the As atoms, large white balls are the Ga atoms, and large dark balls are the Mn atoms. Subscripts refer to an As-terminated (001)- $2 \times 2$  surface, thus  $\gamma_{102}$  represents adding one Mn and one As-As dimer.  $\beta_{100}$  represents adding one Mn.  $\beta_{140}$  represents adding four Ga to first form a Ga-terminated surface, and then adding a Mn.  $\alpha_{202}$  represents adding two Mn-As dimers.  $\beta_{21-1}$  represents replacing a surface As by a Ga and then adding two Mn.  $\alpha_{220}$  represents adding two Mn-Ga dimers.  $\gamma_{300}$  represents adding three Mn.  $\beta_{40-1}$  represents adding four Mn while creating one As vacancy (denoted by the dashed-line squares).

the lowest unoccupied molecular orbital (LUMO) states of about 1.0 eV, as measured at the special  $k$  points used in the Brillouin-zone sum.

The next low-energy structures are the  $\beta$  phases where the Mn assumes an interstitial position (see, for example, the  $\beta_{100}$  phase in Fig. 3) in an  $sd^3$  hybrid. It has four As nearest neighbors, as depicted in Fig. 1(b). In  $\beta_{100}$ , the Mn atom is located below the As-As dimers, whereas in  $\beta_{140}$  (see Fig. 3), the Mn atom is located in the trough between the Ga-Ga dimers, and is hence with four Ga nearest neighbors. The band gaps are 0.8 and 0.9 eV for  $\beta_{100}$  and  $\beta_{140}$ , respectively.

For conventional semiconductor surfaces, the existence of an energy gap lays the ground for the EC model<sup>8</sup> in which each atom contributes a nominal fractional charge [= (number of valence electron)/(number of bonds)] to each of the shared and dangling bonds. To facilitate the energy minimization process dictated by this model, the charge transfer occurs between atoms so that all shared bonds and low-lying dangling bonds are fully occupied and all high-lying dangling bonds are empty. Here, to a first-order approximation, Mn provides two  $s$  valence electrons to the ( $s,p$ )-bonding network, leaving five  $d$  electrons intact. Thus, the  $\gamma$  motif contributes one-half of an electron to each of the

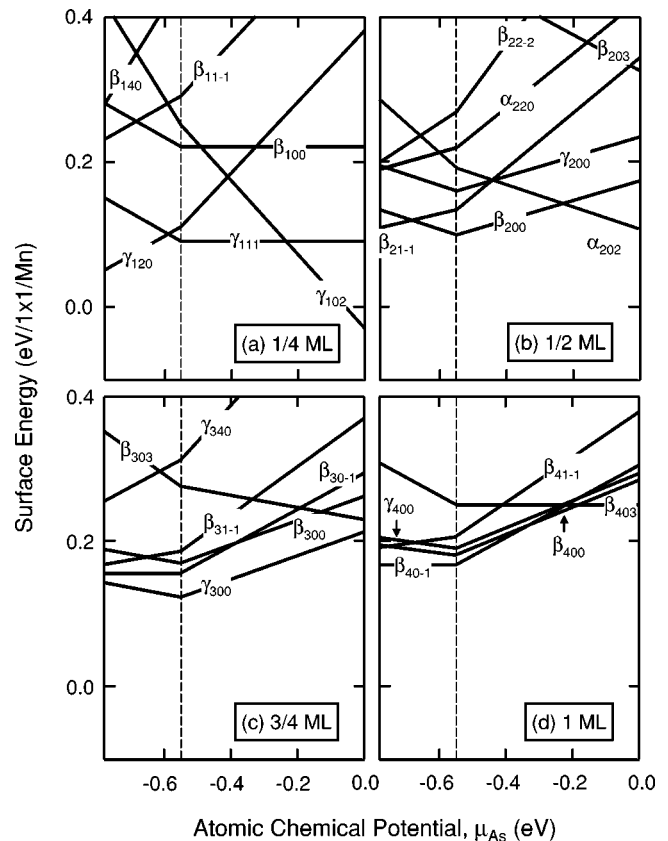


FIG. 4. Calculated surface energies as a function of the As chemical potential: on the horizontal axis,  $\mu_{As}=0$  corresponds to the As-rich whereas  $\mu_{As}=-0.78$  eV corresponds to the As-poor condition. The cusps at the vertical dashed line are a result of Eq. (4).

four Mn-As bonds, whereas the  $\beta$  motif is merely a double donor ( $2+$ ), so the EC model holds at this particular Mn coverage.

$\theta_{Mn}=1/2$  ML. Here, both the  $\beta$  and  $\gamma$  phases are antiferromagnetic (AFM), so  $M_T=0$ . The  $\beta_{200}$  phase has lower energy than the  $\gamma_{200}$  phase, in which two Mn atoms replace all four surface Ga atoms. The energy difference between the AFM and the ferromagnetic (FM) arrangements is 0.3 eV/Mn for the  $\beta$  phases, but is smaller, only 0.13 eV/Mn, for the  $\gamma$  phase. The AFM arrangement is favored here because it allows for a gap between the HOMO and LUMO states, e.g., about 1.1 eV for the  $\beta$  phases and 1.0 eV for the  $\gamma$  phase. In contrast in the FM arrangement, the spin-up HOMO state is pushed up by about 0.5 eV with respect to that of AFM, whereas the spin-down LUMO state is pushed down by about 0.3 eV. This results in a diminishing gap and hence higher surface energy. The large AFM energy of the  $\beta$  phases over that of the  $\gamma$  phases account for the switchover between  $\beta$  and  $\gamma$ . By comparing Figs. 4(a) and 4(b), we see that two separate Mn in the  $\beta$  motif would like to form an AFM pair with about 0.1 eV/Mn binding energy. As such, the previous model<sup>13</sup> regarding Mn incorporation via isolated  $\beta$  motifs should be reexamined.

$\theta_{Mn}=3/4$  ML. Here, as a result of the partial AFM arrangement of the Mn spins,  $M_T=5\mu_B/2 \times 2$ . The  $\gamma_{300}$  phase

has the lowest energy. Due to a strain effect, however, one of the Mn atoms in  $\gamma_{300}$  has two Ga and two As nearest neighbors, instead of the four As nearest neighbors in Fig. 1(c). The gaps at  $\theta_{\text{Mn}}=3/4$  ML are smaller than those at  $\theta_{\text{Mn}}\leq 1/2$  ML, 0.8 eV for  $\gamma_{300}$ , and zero for  $\beta_{300}$ . Evidently, the vanishing gap for  $\beta_{300}$  is an important factor for the switch-back from  $\beta$  to  $\gamma$ . Also, surfaces with vacancies are energetically favored at this coverage, e.g.,  $\beta_{30-1}$  with a Ga vacancy is more stable than  $\beta_{31-1}$  without the vacancy, which is, however, not the case at  $\theta_{\text{Mn}}\leq 1/2$  ML.

$\theta_{\text{Mn}}=1$  ML. Here,  $M_T=0$  and all the surfaces in Fig. 4(d) are metallic, so the semiconductor-to-metal transition is complete at  $\theta_{\text{Mn}}=1$  ML. The AFM energies for the  $\beta$  phases are smaller but still significant, 0.1 eV/Mn, so they have lower energies. Due to the metallicity, however, the energy difference between different reconstructions is reduced with respect to  $\theta_{\text{Mn}}<1$  ML. The energy of the (Mn, double-As-layer) surface, which is high at low  $\theta_{\text{Mn}}$  [e.g.,  $\beta_{203}$  in Fig. 4(b)], steadily decreases with  $\theta_{\text{Mn}}$ . At 1 ML,  $\beta_{403}$  has the lowest energy at the As-rich limit, indicative of the transition to MnAs epitaxy.

The experimental results in Fig. 2(a) showed that surfaces with low Mn coverage are segregated into the  $2\times 4$  areas and the depressed  $2\times 2$  areas that grow at higher Mn coverage. To account for such segregation, one should compare the energy per unit area *per Mn*, as in Fig. 4. Also, annealing without an As ambient pressure usually results in the loss of surface As atoms. Hence, we will consider the  $\gamma_{120}$  (1/4 ML),  $\beta_{21-1}$  (1/2 ML),  $\gamma_{300}$  (3/4 ML), and  $\beta_{40-1}$  (1 ML) surfaces at  $\mu_{\text{As}}=-0.78$  eV in Fig. 4. Although we have not been able to experimentally determine  $\theta_{\text{Mn}}$ , it is highly likely that the experiments were done for nonequilibrium surfaces, as pro-

longed annealing at 590 °C will destroy the  $2\times 2$  pattern. Growth kinetics is therefore important. Forming the  $\beta$  surfaces during annealing is kinetically more feasible than forming the others, because the former only requires the Mn diffusion on the surface and through the surface As-As dimers with a negligibly small 0.2-eV energy barrier.<sup>13</sup> Most importantly, the calculated STM image for the  $\beta_{40-1}$  surface at the  $-2$  V bias in Fig. 2(c) agrees with the experiment in Fig. 2(b): The highest As atom is pushed upward by the underlying Mn by about 0.5 Å. This translates into a depressed area  $2.8-0.5=2.3$  Å below the top surface, in good agreement with experiment (2.2 Å). In contrast, the calculated STM image for the  $\gamma$  motif (not shown) is featureless due to its planar structure and, hence, disagrees with experiment.

In summary, we have systematically studied spin-driven reconstructions on GaAs(001)- $2\times 2$ :Mn. A structural-motif-based theory for transition-metal-covered semiconductor surface reconstructions is developed: The magnetic spins manifest themselves through antiferromagnetic couplings in order to maintain semiconducting band gaps and hence low surface energies. However, at  $\theta_{\text{Mn}}=1$  ML, the gaps close and the semiconductor-to-metal transition takes place. The calculated STM images agree with experiment, revealing the identity of the observed  $2\times 2$  surfaces.

S.B.Z. was supported by the U.S. DOE/BES and DOE/EERE under Contract No. DE-AC36-99GO10337 and by the NERSC for MPP time. Work at IOP was supported by the grants from NSF (Nos. 60021403, 10134030), and MOST (Nos. G2000067103, G001CB3095, 2002AA311151) of China.

<sup>1</sup>H. Ohno, *Science* **281**, 951 (1998).

<sup>2</sup>T. Dietl, H. Ohno, F. Matsukura, J. Cibert, and D. Ferrand, *Science* **287**, 1019 (2000).

<sup>3</sup>S. A. Wolf, D. D. Awschalom, R. A. Buhrman, J. M. Daughton, S. von Molnár, M. L. Roukes, A. Y. Chtchelkanova, and D. M. Treger, *Science* **294**, 1488 (2001).

<sup>4</sup>H. Ohno, F. Matsukura, and Y. Ohno, *JSAP International* **5**, 4 (2002).

<sup>5</sup>J. E. Northrup and S. Froyen, *Phys. Rev. Lett.* **71**, 2276 (1993).

<sup>6</sup>Q. K. Xue, T. Hashizume, and T. Sakurai, *Prog. Surf. Sci.* **56**, 1 (1997).

<sup>7</sup>S. B. Zhang and A. Zunger, *Phys. Rev. B* **53**, 1343 (1996).

<sup>8</sup>M. D. Pashley, *Phys. Rev. B* **40**, 10481 (1989).

<sup>9</sup>A. Janotti, S.-H. Wei, and L. Bellaiche, *Appl. Phys. Lett.* **82**, 766 (2003).

<sup>10</sup>E. J. Singley, R. Kawakami, D. D. Awschalom, and D. N. Basov, *Phys. Rev. Lett.* **89**, 097203 (2002).

<sup>11</sup>K. M. Yu, W. Walukiewicz, T. Wojtowicz, I. Kuryliszyn, X. Liu, Y. Sasaki, and J. K. Furdyna, *Phys. Rev. B* **65**, 201303 (2002).

<sup>12</sup>P. A. Korzhavyi, I. A. Abrikosov, E. A. Smirnova, L. Bergqvist, P. Mohn, R. Mathieu, P. Svedlindh, J. Sadowski, E. I. Isaev, Yu.

Kh. Vekilov, and O. Eriksson, *Phys. Rev. Lett.* **88**, 187202 (2002).

<sup>13</sup>S. C. Erwin and A. G. Petukhov, *Phys. Rev. Lett.* **89**, 227201 (2002).

<sup>14</sup>X. Jin, M. Zhang, G. S. Dong, Y. Chen, M. Xu, X. G. Zhu, Xun Wang, E. D. Lu, H. B. Pan, P. S. Xu, X. Y. Zhang, and C. Y. Fan, *Phys. Rev. B* **50**, 9585 (1994).

<sup>15</sup>Z. Yang, K. Zhang, S. Ke, and X. Xie, *Phys. Rev. B* **56**, 6727 (1997).

<sup>16</sup>P. Hohenberg and W. Kohn, *Phys. Rev.* **136**, B864 (1964); W. Kohn and L. J. Sham, *Phys. Rev.* **140**, A1133 (1965).

<sup>17</sup>J. P. Perdew and Y. Wang, *Phys. Rev. B* **33**, 8800 (1986).

<sup>18</sup>D. Vanderbilt, *Phys. Rev. B* **32**, 8412 (1985).

<sup>19</sup>G. Kresse and J. Hafner, *Phys. Rev. B* **47**, 558 (1993); G. Kresse and J. Furthmüller, *ibid.* **54**, 11169 (1996).

<sup>20</sup>G. Qian, R. M. Martin, and D. J. Chadi, *Phys. Rev. B* **38**, 7649 (1988).

<sup>21</sup>Bulk Mn has a complex ground-state atomic structure. In this study, we used an antiferromagnetic fcc structure.

<sup>22</sup>Detailed account of the experimental observations will be published elsewhere. Different from Ref. 14, however, we did not observe the  $4\times 1$  reconstruction measured by LEED.